The first ADC bearing the ferroptosis inducer RSL3 as a payload with conservation of the fragile electrophilic warhead

Kim-Anh Nguyen, Louise Conilh, Pierre Falson, Charles Dumontet, Ahcène Boumendjel

The first ADC bearing the ferroptosis inducer RSL3 as a payload with conservation of the fragile electrophilic warhead

Kim-Anh Nguyen [a,1], Louise Conilh [b,1], Pierre Falson [c], Charles Dumontet [b,d,2], Ahc`ene Boumendjel [a,*,2]

[a] University of Grenoble Alpes, INSERM, LRB, 38000, Grenoble, France
[b] Cancer Research Center of Lyon (CRCL), INSERM, 1052/CNRS, 5286/UCBL, 69000, Lyon, France
[c] Drug Resistance and Membrane Proteins Group, Molecular Microbiology and Structural Biochemistry Laboratory, CNRS UMR 5086, University of Lyon, IBCP, 7, Passage du Vercors, 69367, Lyon, France [d] Hospices Civils de Lyon, 69000, Lyon, France

ARTICLEINFO

Keywords:
Antibody-Drug conjugates
ADC
Ferroptosis
Ferroptosis inducer
GPX4
RSL3

ABSTRACT

The iron-dependent, non-apoptotic cell death, known as ferroptosis is an emerging strategy for the development of anticancer drugs. RSL3 was identified as an activator of ferroptosis through the inhibition of the glutathione peroxidase 4 (GPX4) which plays a crucial role in the cellular lipid oxidative stress. RSL3 is characterized by the presence of an electrophilic chloroacetyl moiety, namely warhead which covalently bonds to the catalytic and nucleophilic selenocysteine residue (Sec46) of GPX4. Like the major ferroptosis inducers, RSL3 suffers from lack of selectivity toward tumor cells. In this study, we report the first synthesis of an antibody-drug conjugate (ADC) containing RSL3 fragment and trastuzumab with the aim to deliver the agent selectively to tumors. The synthesis uses a judiciously chosen strategy to preserve the vital but fragile warhead. Full characterization of the ADC was accomplished, demonstrating the generation of a homogeneous DAR 8 conjugate. The robustness of the synthesis was successfully applied to another ADC associating the anti-CD74 mAb milatuzumab. The ADC induces ferroptotic cell death through reactive oxygen species accumulation and increases the activity of doxorubicin. The ADC associating trastuzumab and RSL3 may therefore offer potential applications in vectorized therapy alone or in combination with conventional chemotherapies.

1. Introduction

Reported in 2012, ferroptosis is an iron-dependent form of non- apoptotic regulated cell death which is distinct from other types of cell death, including apoptosis, necrosis, and autophagy [1]. Ferroptosis leads to large amount of iron accumulation and lipid peroxidation in the cell and ultimately to cell death. It is tightly linked to glutathione peroxidase 4 (GPX4) which plays a key role in the dissipation of cellular lipid oxidative stress and reduction of lipid hydroperoxides [1,2]. The enzyme reduce organic and inorganic hydroperoxides to the corresponding alcohols employing reduced glutathione (GSH) as electron donor [3,4]. It was established that activators of ferroptosis induce a decrease in the antioxidant potential of cells and accumulation of lipid reactive oxygen species (ROS), leading to oxidative cell death [5]. Hence, the inhibition of GPX4 enzymatic function is considered to be a valuable strategy to induce ferroptosis and kill cancer cells [5,6]. In this context, several GPX4 inhibitors have been developed. These inhibitors are characterized by the presence of an electrophilic chemical entity, namely warhead which covalently bonds to the catalytic and nucleophilic selenocysteine residue (Sec46) present in the active site of human GPX4. Different warheads have been embedded on inhibitors, such as chloroacetamides [3,7–9]. Among the chloroacetamide-containing inhibitors identified so far, RSL3 is considered to be the GPX4-targeting pioneer that has been used to conceive alternative classes of compounds, including ML62 and DP117 (Fig. 1) [3,7–9]. Interestingly, Schreiber and co-workers have reported that diacylfuroxans as novel generation of inhibitors of GPX4 by acting as prodrugs through the generation of electrophilic masked nitrile oxides (Fig. 1) [10–12].

Despite their effectiveness, GPX4-inhibitors suffer from the lack of selectivity [2]. One strategy to overcome the selectivity challenge could be the vector-based chemotherapy that allows the selective delivery of the ferroptosis inducer within a tumor. The development of an antibody-drug conjugate (mAb) combining a ferroptosis inducer and the antigen specificity and long circulating half-life of the mAb could be an interesting strategy to target ferroptosis more effectively [13]. Antibody–drug conjugates (ADCs) have made considerable progress within the last two decades [14]. The ADC concept takes advantage of the specific binding properties of monoclonal antibodies (mAb) to biological targets to selectively deliver small-molecule drugs [13]. Typically, an ADC results from the coupling of a small molecule to a mAb *via* a chemical linker that can be cleaved near or at the cellular target. The first ADC approved by the FDA in 2009 was Mylotarg® [13]. In 2021, no less than eleven ADCs were approved, witnessing to the importance of targeted therapy, particularly for oncology [14]. However, it is noteworthy that the ADC field is heavily dominated by tubulin inhibitors, such as auristatins and maytansinoids [14].

Herein, we report the first ADC associating RSL3 and trastuzumab, dealing with the challenge to preserve the chloroacetamide warhead which is highly sensitive to nucleophilic attacks. The full characterization of the ADC and first in vitro results are reported.

2. Results and discussion

2.1. Chemistry

2.1.1. Synthesis of trastuzumab-RSL3-NH_2

The structure of the designed ADC is shown below (Fig. 2). The first component of the ADC is RSL3-NH_2, a very close analog of RSL3 in which an amino moiety was introduced to replace the ester group present at the

Abbreviations: ADC, antibody-drug conjugate; DAR, drug-to-antibody ratio; GPX4, glutathione peroxidase 4; mAb, monoclonal antibody; ROS, reactive oxygen species.

* Corresponding author.
E-mail address: ahcene.boumendjel@univ-grenoble-alpes.fr (A. Boumendjel).

[1] These authors contributed equally to this work.
[2] These authors contributed equally to this work.

https://doi.org/10.1016/j.ejmech.2022.114863

Received 11 September 2022; Received in revised form 14 October 2022; Accepted 18 October 2022 Available online 29 October 2022

aromatic ring, unnecessary for the ferroptosis activity [2]. The dipeptide Ala-Val bearing an azido group was used as an intracellular protease-cleavable linker, which can be attached to RSL3-NH_2 via peptide coupling. The third component is the trastuzumab functionalized with dibenzylcyclooctyne (DBCO) that can be coupled to the linker Ala-Val-N_3 through click chemistry [15]. It is worth noting that the RSL3-NH_2 must maintain the 1*S*,3*R* configuration of RSL3, that is essential for the ferroptosis activity [14]. The synthesis strategy was based on a sequence in which the chloroacetamide was introduced at a late stage of the synthetic scheme to avoid the highly probable chlorine displacement in the presence of nucleophiles.

The synthesis of the precursors (**1** and **2**) required for the preparation of the RSL3-NH-Ala-Val fragment is shown in Scheme 1. The synthesis and analysis details are provided in the supporting information section.

The next step deals with the coupling of **1** and **2** under peptide coupling conditions (Scheme 2). The obtained derivative **7** was subjected to acidic Boc-deprotection and reaction of the resulting compound with chloroacetyl chloride to afford compound **8**. High care was taken during the work-up and purification procedures to conserve the chloroacetyl moiety which is highly sensitive to hydrolysis during the work-up step.

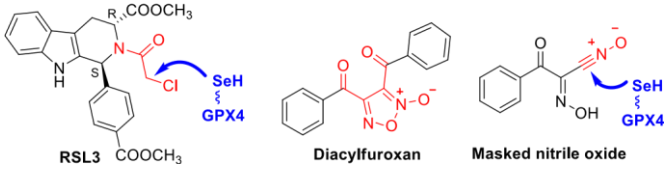

Fig. 1. Structure of RSL3 bearing a chloroacetamide warhead [3], and masked nitrile oxide derived from diacylfuroxan [10] and their reaction with the nucleophilic selenocysteine residue of GPX4.

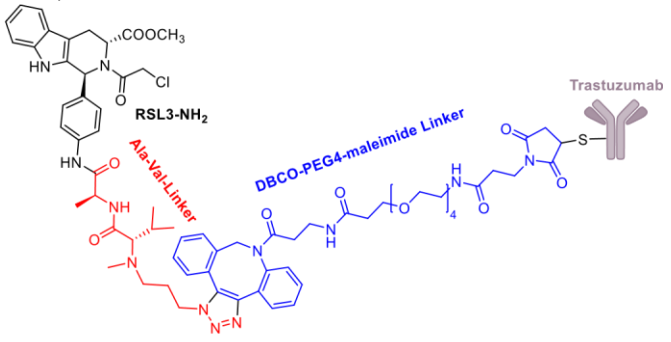

Fig. 2. Structure of the designed ADC.

The synthesis of the trastuzumab-DBCO conjugate (precursor **3**) was carried out in two steps (Scheme 3) [16–18]. First, trastuzumab was subjected to reduction conditions with TCEP in the presence of EDTA in order to reduce the interchain disulfide bonds. The next step was the addition of the free thiols in the reduced mAb to the maleimide moiety of the commercially available dibenzocyclooctyne-PEG4-maleimide (DBCO-PEG4-maleimide) (**9**) to provide the precursor **3**. It should be mentioned that the full reduction of the disulfide bonds is highly dependent on the TCEP amounts used (see Experimental section). In the final step, the precursor **8** bearing an azido group was reacted with the cyclooctyne moiety of **3** to form triazole cycloadducts via strain-promoted azide–alkyne cycloaddition (SPAAC). Trastuzumab-RSL3-NH_2 conjugates were purified using Amicon ultracentifugal filters 30K as described previously [19].

2.1.2. Characterization of trastuzumab-RSL3-NH_2

Usual ADCs have generally a DAR (drug-to-antibody ratio) of 2–4 that are appropriate to limit aggregation, activity loss and toxicity caused by the drug-linker hydrophobicity. In the case of RSL3, since it is less cytotoxic than gold standard MMAE or DM1 payloads, a maximum cysteine-conjugated ADC of DAR 8 would enhance the potency. In this regard, few examples of ADCs bearing high DARs were reported in literature, including Enhertu® and Trodelvy® [20]. In the present case, it can be hypothesized that the hydrophilic PEG4 moiety within the drug-linker can limit the hydrophobicity of the ADC. After purification, DAR was measured by denaturing reverse phase liquid chromatography coupled to mass spectrometry (RPLC-MS) as described before [19]. The results confirmed the obtaining of a homogeneous ADC with an average DAR of 7.9, exhibiting a majority of fully conjugated light chains (deconvoluted LC+1 Calc: 24793 Da; Obs: 24792.8 Da) and heavy chains (deconvoluted HC+3 calc: 54656 Da; Obs: 54655.5 Da) (Fig. 3A). Similar to unconjugated trastuzumab, our ADC presented a majority of the G0F glycoform. Since no difference was observed between calculated and observed masses for either the light or the heavy chains, no degradation of either the mAb or the drug-linker has occurred. The mass spectrometry data confirmed the preservation of the chloroacetamide warhead that is mandatory for the ferroptosis activity. In order to expand the bioconjugation method, we generated another ADC comprised of the anti-CD74 mAb milatuzumab and RSL3-NH_2. RPLC-MS analysis confirmed the generation of a DAR 7.9 ADC bearing intact chloroacetamide group (see Supplementary data, Fig. S2). Moreover, we verified the monomeric purity and non-aggregated aspect of trastuzumab-RSL3-NH_2 by size exclusion chromatography (SEC) (Fig. 3B). Taken together, these results indicate that the bioconjugation strategy can generate highly conjugated, homogeneous and monomeric RSL3-NH_2-based ADCs, independently of the mAb, and therefore the target cells.

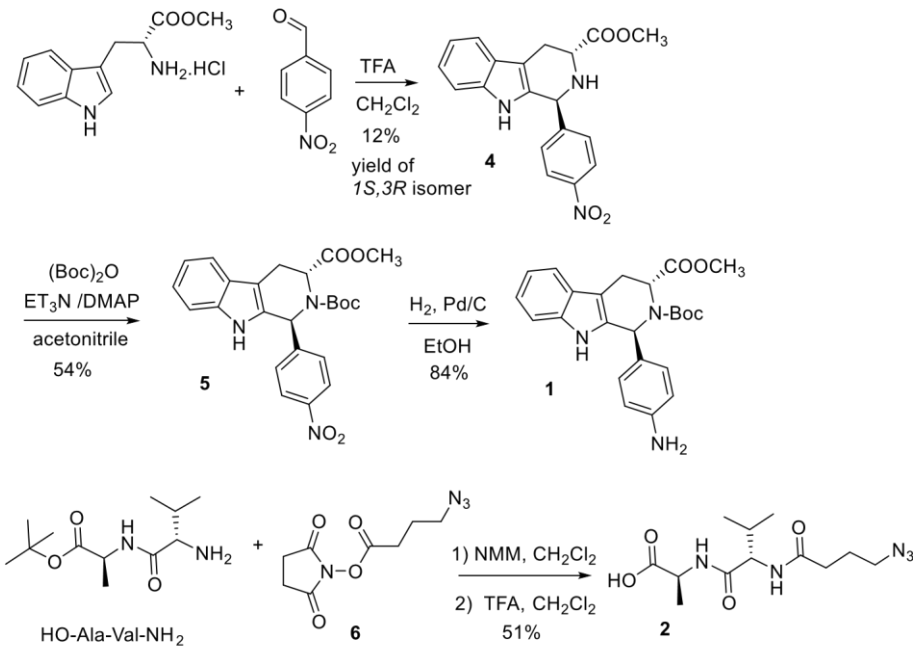

Scheme 1. Synthesis of precursors **1** and **2**.

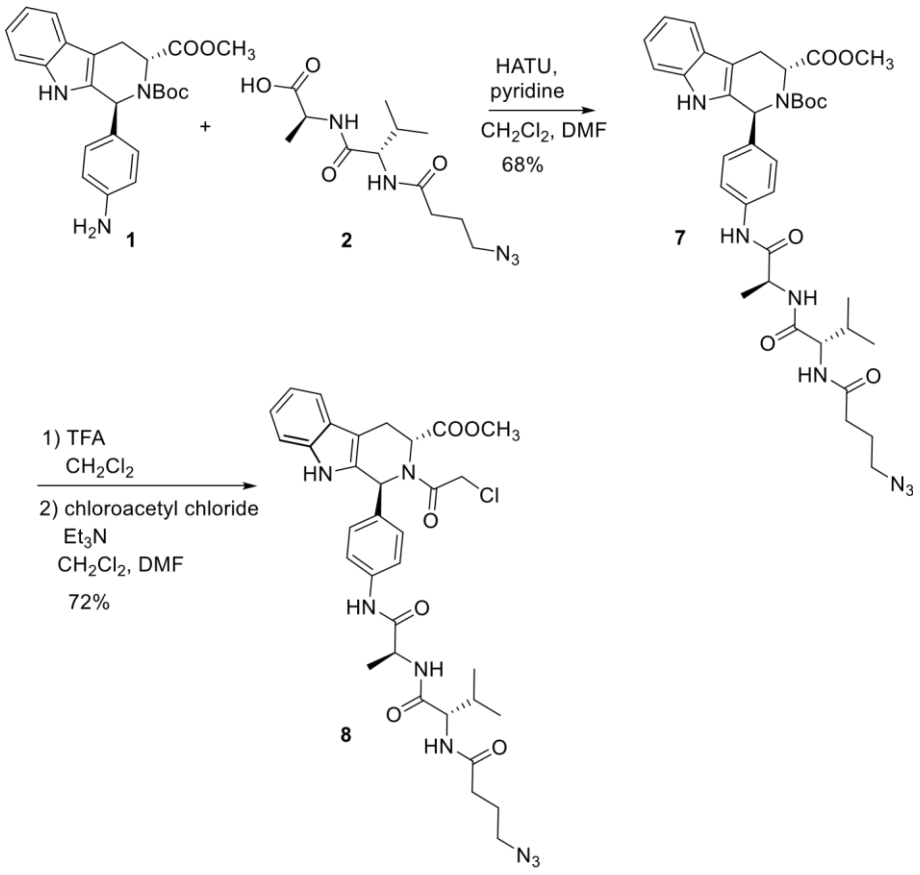

Scheme 2. Synthesis of compound **8**.

2.2. Biological evaluation

HER2-positive cell line BT-474 was strongly sensitive to RSL3 and

2.2.1. In vitro evaluation of RSL3 and RSL3-NH₂

(Supplementary data, Fig. S3B) to identify RSL3-sensitive cell lines. The therefore selected for further in vitro studies. In addition, the cytotox-

The cytotoxicity of RSL3 was assessed by the MTT (3-(4,5-dime- icity of RSL3-NH_2 and its (1*R*,3*R*) isomer (compounds **S11** and **S13**, thylthiazol-2-yl)-2,5-diphenyltetrazolium bromide)) cytotoxicity assay Supplementary data) was evaluated by the MTT cytotoxicity assay in

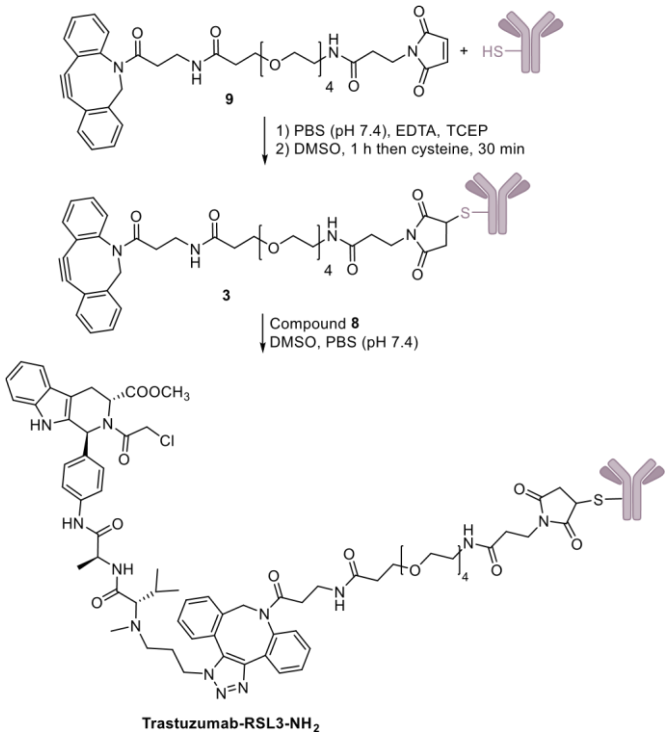

Scheme 3. Preparation of trastuzumab-RSL3-NH_2 conjugates.

numerous cell lines and compared to RSL3 (Supplementary data, Fig. S3C). The measured IC_{50} demonstrated a ten-time loss of cytotoxic activity of RSL3-NH_2 compared to RSL3. The artificial membrane permeability assay (PAMPA) demonstrated a nearly tenfold decrease in membrane passive diffusion of RSL3-NH_2 compared to RSL3 (Supplementary data, Fig. S3D), explaining the weaker cytotoxicity of RSL3- NH_2, given that the amino group of this compound can be protonated and positively charged. As expected, the cytotoxicity of (1*R*,3*R*)-RSL3- NH_2 was even lower (100-times) suggesting that the configuration of (1*S*,3*R*) is critical for the activity. We therefore had to ensure that RSL3- NH_2, once released within the target cells, could inhibit GPX4 and consequently, trigger ferroptosis with comparable efficacy to RSL3. Hence, binding capacity of RSL3-NH_2 to GPX4 was evaluated by gel mobility shift Western blot as previously described [14]. Treatment of the GPX4-expressing BT-474 cell line with RSL3-NH_2 resulted to a shift of GPX4, as observed with RSL3, indicating that RSL3-NH_2 is an irreversible inhibitor of GPX4 (Fig. 4A). A hallmark of ferroptosis is the accumulation of ROS and specifically to lipid peroxides to a lethal dose and GPX4 is an essential protein participating in the lipid hydroperoxides and ROS elimination pathway [7]. On the one hand, ROS accumulation induced by RSL3-NH_2 was quantified using the ROS indicator H2D-CFDA. On the other hand, lipid peroxidation was evaluated using the lipid peroxidation sensor Bodipy c11 581/591. The results showed a strong increase in ROS levels and similarly, lipid peroxides content when cells were treated with either RSL3 or RSL3-NH_2 compared to non-treated cells (Fig. 4B and C). In addition, cells co-treated with RSL3 or RSL3-NH_2 and the lipophilic antioxidant and ROS scavenger ferrostatin-1 (Fer-1) demonstrated a restored ROS content and in the same way, lipid peroxides content (Fig. 4B and C). In addition, the presence of the antioxidant Fer-1 rescued cells from RSL3-or RSL3-NH_2-induced cell death (Fig. 4D), confirming that RSL3-NH_2 triggers ferroptosis.

These results indicate that RSL3-NH_2 is able to irreversibly inhibit GPX4, induce ROS and lipid peroxides accumulation and trigger ferroptosis, comparable to RSL3. These findings also validated our approach to design the trastuzumab-RSL3-NH_2 conjugate.

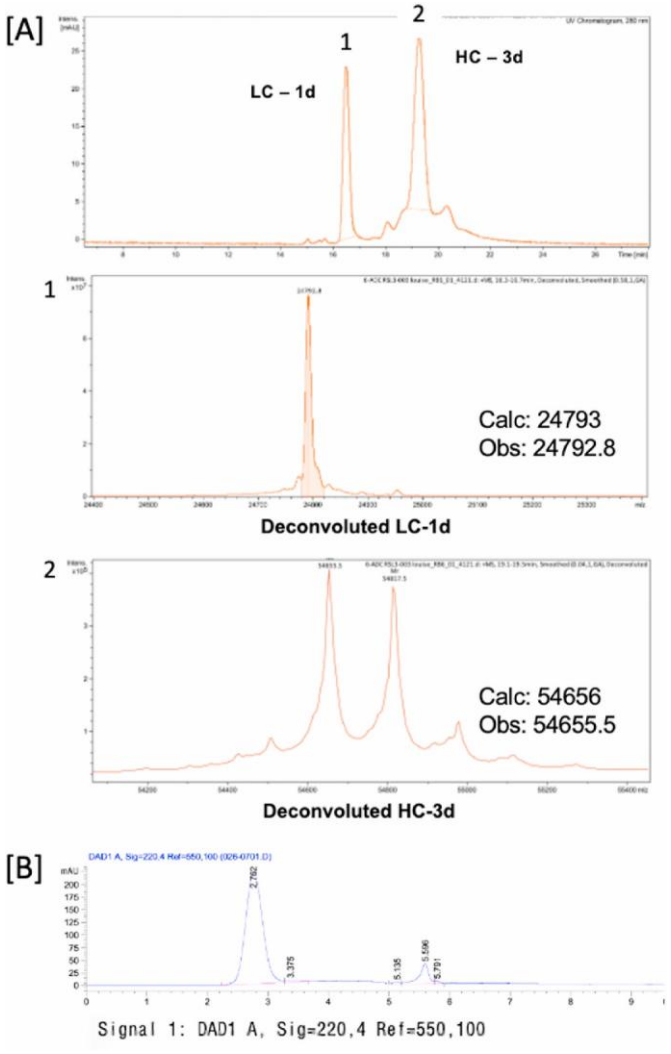

Fig. 3. Physicochemical characterization of trastuzumab-RSL3-NH_2. [A] RPLC- QToF profile of trastuzumab-RSL3-NH_2, displaying deconvoluted profiles: peak 1 corresponds to the LC-1d; peak 2 corresponds to HC-3d. Calculated masses were obtained as the sum of trastuzumab LC or HC molecular weight plus one (LC-1d) or three (HC-3d) drug-linker molecular weight. [B] The monomeric purity and non-aggregated aspect of trastuzumab-RSL3-NH_2 verification by size exclusion chromatography (SEC).

2.2.2. In vitro evaluation of trastuzumab-RSL3-NH_2

Trastuzumab-based ADCs deliver their payloads into cells through endocytosis after binding to the receptor HER2. Hence, we needed to evaluate the antigen binding capacity of our ADC by indirect ELISA binding assay (Fig. 5A). The unconjugated and conjugated forms of trastuzumab demonstrated log(EC_{50}) values of − 8.81 and − 8.87, respectively, indicating maintained HER2 binding capacity of trastuzumab while highly conjugated to RSL3-NH_2. Moreover, MTT cytotoxicity assay in the HER2-positive cell line BT-474 demonstrated a higher cytotoxicity of the ADC compared to the naked trastuzumab (Fig. 5B). Similarly, milatuzumab-RSL3-NH_2 exhibited a strong cytotoxicity (IC_{50} = 2.4 nM) against the CD74-positive cell line Toledo (Supplementary data, Fig. S4).

Next, we set out to confirm whether the ADC, like RSL3-NH_2 and RSL3, induced cell death via ferroptosis. Hence, treatment of BT-474 cells with the ADC induced increased lipid peroxidation as quantified with Bodipy c11 581/591, which was correlated with cell death (Fig. 5C). When BT-474 cells were co-treated with trastuzumab-RSL3- NH_2 and the antioxidant Fer-1, lipid peroxides content was restored, and

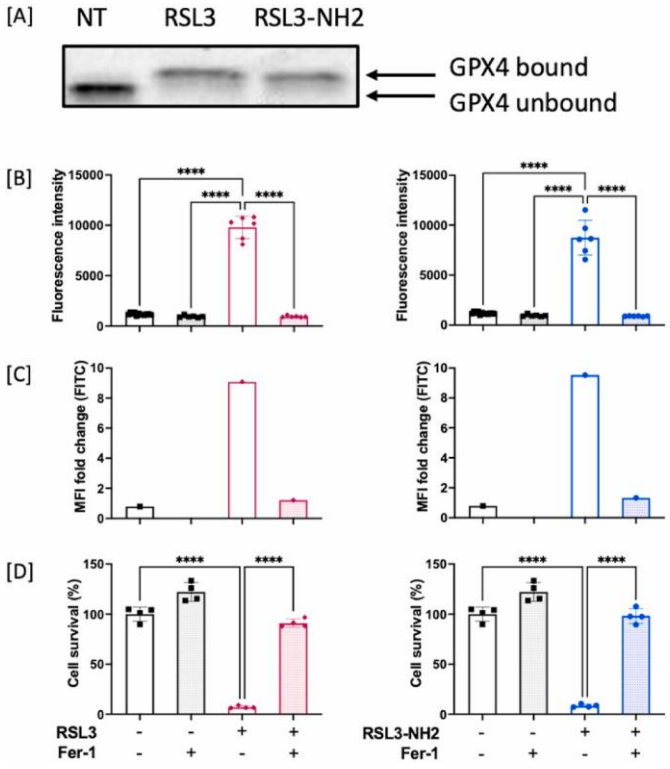

Fig. 4. *In vitro* evaluation of RSL3 and RSL3-NH_2. [A] Gel shift assay of GPX4 in BT-474 cells by RSL3 (2 µM) or RSL3-NH_2 (10 µM) after 18h incubation. [B] ROS quantification by H2D-CFDA of BT-474 cancer cell line treated with RSL3 (1 µM) or RSL3-NH_2 (10 µM) alone or in combination with the antioxidant Fer-1 (2 µM) for 1 h. [C] Lipid peroxidation capacity quantification using Bodipy c11 581/591 of BT-474 treated with RSL3 (10 µM) or RSL3-NH_2 (10 µM) alone or in combination with Fer-1 (2 µM) for 1 h. [D] Cytotoxicity evaluation by MTT BT- 474 treated with RSL3 (1 µM) or RSL3-NH_2 (10 µM) alone or in combination with Fer-1 (2 µM) for 72 h. Data are presented as mean + S/D of a single experiment containing four or more technical replicates, representative of independent experiments. Significance was determined by ordinary one-way ANOVA, *p < 0.05, **p < 0.01, ***p < 0.001, ****p < 0.0001.

cell viability was significantly reduced compared to cells treated with trastuzumab-RSL3-NH_2 alone (Fig. 5C). However, the partly restoration of cell viability showed that both apoptosis, induced by HER2 inhibition, and ferroptosis, triggered by GPX4 inhibition, were responsible for cancer cell death.

Studies have demonstrated a strong synergy potential between ferroptosis inducers and standard chemotherapeutic agents [21–23]. Hence, ROS levels within the breast cancer cell line BT-474 were investigated after RSL3 or RSL3-NH_2 treatment alone or in combination with doxorubicin (Supplementary data, Figs. S5A and B). Both RSL3 and RSL3-NH_2 induced significant ROS formation, compared to non-treated cells, as previously observed, while doxorubicin did not after 1 h of treatment. However, doxorubicin combined with either RSL3 or RSL3-NH_2 led to an increase in ROS content. Cell viability also decreased when cells were co-treated with RSL3 plus doxorubicin (Supplementary data, Fig. S5C). This correlation between ROS content and cell viability suggests that a combined treatment of doxorubicin and a GPX4 inhibitor could sensibilize cancer cells to ferroptosis.

The HER2-positive SKBR-3 and NCI–N87 cell lines were not sensitive to either RSL3 or RSL3-NH_2 treatment (Supplementary data, Fig. S3B). However, when these cell lines were treated with doxorubicin together with the ADC, cell viability was reduced (Fig. 5D and Fig. S5D, Supplementary data). It should be mentioned that the cell death was less pronounced when treated with trastuzumab alone. Thus, cells initially resistant to ferroptosis could be sensibilized to GPX4 inhibitors by combining them with doxorubicin.

3. Conclusions

Ferroptosis is characterized by a large amount of iron accumulation and lipid peroxidation within the cell. The ferroptosis inducers are emerging as novel agents to be developed as new generation of cytotoxics. We reported here the first monomeric, and homogeneous conjugate of trastuzumab bearing eight units of a ferroptosis inducer, (1*S*,3*R*)-RSL3-NH_2. The conjugation method was meticulously designed in order to preserve the chloroacetamide warhead of the active drug, especially during the last-stage click reaction. The robustness of the synthetic method was confirmed with a second mAb. Both drug analog (RSL3-NH_2) and the resulting ADC maintained GPX4 inhibition, resulting in a significant augmentation of ROS content and ultimately ferroptotic cell death in the same manner as RSL3. The conjugation with trastuzumab not only delivers RSL3-NH_2 to the target cancer cells, but also helps RSL3-NH_2 to overcome membrane permeability issues via endocytosis. Moreover, the combination of a kinase targeting mAb and a GPX4 inhibitor displayed synergistic cytotoxicity via both ferroptosis and apoptosis. In addition, cells initially resistant to ferroptosis inducers like RSL3-NH_2 were re-sensibilized by combining the ADC with doxorubicin, resulting in increased cytotoxicity. The synthetic chemistry and the biological results reported here established a strong molecular foundation for warranting exciting *in vivo* studies of the first ADC bearing a ferroptosis inducer [24].

4. Experimental section

4.1. Chemistry

Commercially available reagents and solvents were purchased and used without further purification. Reactions were monitored by thin layer chromatography (plates coated with silica gel 60 F254 from Macherey-Nagel). Products were purified with column chromatography on Silica gel 60 (230–400 mesh from Macherey-Nagel) or by automatic flash chromatography with a Grace device: Reveleris X2. NMR spectra were performed on the NMR-ICMG platform of Grenoble with either on a 400 MHz Bruker Avance-400 instrument (400 MHz) or on a 500 MHz Bruker Avance-500 instrument (500 MHz) at room temperature. Chemical shifts (δ) are reported in parts per million (ppm) relative to TMS as internal standard or relative to the solvent [^{1}H: $\delta(CDCl_3)$ = 7.26 ppm, $\delta(CD_3OD)$ = 3.31 ppm δ(DMSO-d_6) = 2.50 ppm, δ(acetone-d_6) = 2.05 ppm; ^{13}C: $\delta(CDCl_3)$ = 77.06 ppm, $\delta(CD_3OD)$ = 49.03 ppm, δ(DMSO-d_6) = 39.53 ppm, δ(acetone-d_6) = 29.82 ppm]. Electrospray ionization ESI mass spectra were acquired by the ICMG platform of Grenoble on an Esquire 3000 Plus Bruker Daltonis instrument with a nanospray inlet. Accurate mass measurements (HRMS) were carried out on an ESI/QTOF with the Waters Xevo G2-S QTof device.

*4.1.1. Methyl (1S,3R)-1-(4-nitrophenyl)-1,3,4,9-tetrahydropyrido[3,4-b] indole-3-carboxylate (**4**)*

*T*o a suspension of D-tryptophan methyl ester hydrochloride (200 mg, 0.78 mmol, 1.2 eq.) in dichloromethane (DCM) was added NEt_3 (0.12 mL, 86 mg, 0.85 mmol, 1.3 eq.) at room temperature. The mixture was stirred for 1 h and concentrated to give D-tryptophan methyl ester as clear oil, which was dried under vacuum for 10 min. Tryptophan methyl ester, along with activated 4 Å molecular sieves (113 mg), was dissolved in anhydrous DCM. 4-Nitrobenzaldehyde (99 mg, 0.65 mmol, 1 eq.) and TFA (7.5 mg, 5 µL, 0.07 mmol, 0.1 eq.) were added to the reaction mixture and the solution was refluxed for 1 h. Then TFA (224 mg, 0.15 mL, 1.96 mmol, 3 eq.) was added to the solution, and the reaction was allowed to stir under reflux overnight. The reaction mixture was cooled to room temperature and water was added and basified to pH = 8 with 30% NaOH. The organic phase was separated, washed

with brine and dried with Na_2SO_4 and then concentrated to give the crude product. The compound was purified by silica gel chromatography (Cyclohexane/ EtOAc 9:1 to 5:5) to give two separate diastereoisomers with about a ratio of 1*R*,3*R*/1*S*,3*R* = 3/2. The two diastereomers were distinguished by NOESY correlation between H-1 and H-3. The (1*S*,3*R*) isomer was obtained as a yellow solid (66 mg, 0.19 mmol). Yield = 24%. $[C]^{25}_{D}$ - 16.7° (c 0.9, MeOH); R_f = 0.44 (Cyclohexane/EtOAc 5:5). ^{1}H NMR (400 MHz, $CDCl_3$) δ ppm 2.59 (bs, 1H), 3.16 (ddd, *J* = 15.6, 6.5, 1.6 Hz, 1H), 3.28 (ddd, *J* = 15.6, 5.5, 1.3 Hz, 1H), 3.72 (s, 3H), 3.92 (dd, *J* = 6.5, 5.5 Hz, 1H), 5.52 (s, 1H), 7.11–7.22 (m, 2H), 7.24–7.30 (m, 1H), 7.45–7.52 (m, 2H), 7.54–7.59 (m, 1H), 7.62 (s, 1H), 8.13–8.20 (m, 2H). ^{13}C NMR (100 MHz, $CDCl_3$) δ ppm 24.7 (CH_2), 52.4 (CH_3), 52.8 (CH), 54.4 (CH), 109.0 (C), 111.2 (CH), 118.6 (CH), 120.0 (CH), 122.6 (CH), 124.0 (2xCH), 127.0 (C), 129.4 (2xCH), 131.9 (C), 136.4 (C), 147.8 (C), 149.5 (C), 174.1 (C).

*4.1.2. Methyl (1S,3R)-2-(tert-butoxycarbonyl)-1-(4-nitrophenyl)-1,3,4,9-tetrahydropyrido[3,4-b]indole-3-carboxylate (**5**)*

Compound **4** (91 mg, 0.26 mmol, 1 eq.) was dissolved in dry acetonitrile (ACN), along with Et_3N (0.11 mL, 79 mg, 0.78 mmol, 3 eq.) and stirred under argon. Di-*tert*-butyl dicarbonate (0.12 mL, 113 mg, 2 eq.) and 4-(dimethylamino)pyridine (DMAP) (6 mg, 0.05 mmol, 0.2 eq.) were dissolved in ACN and added dropwise to the reaction mixture. The reaction was heated at 50 °C overnight. Upon reaction completion, ACN was removed and the residue was redissolved in DCM. The reaction was quenched by addition of NH_4Cl 2 N. The organic phase was washed with brine and dried with Na_2SO_4. The resulting crude product was purified by column chromatography (Cyclohexane/EtOAc 9:1 to 7:3) to obtain the pure product as a white solid (63 mg, 0.14 mmol, 54% yield). ^{1}H NMR (400 MHz, $CDCl_3$) δ ppm 1.38 (s, 9H), 2.87 (ddd, *J* = 16.1, 11.0, 1.5 Hz, 1H), 3.14 (dd, *J* = 16.1, 4.9 Hz, 1H), 3.51 (dd, *J* = 11.0, 4.9 Hz, 1H), 3.75 (s, 3H), 5.88 (s, 1H), 7.28–7.41 (m, 4H), 7.49–7.54 (m, 1H), 8.11–8.21 (m, 3H). ^{13}C NMR (100 MHz, $CDCl_3$) δ ppm 25.8 (CH_2), 28.1 ($3xCH_3$), 50.3 (CH), 52.4 (CH_3), 55.9 (CH), 84.5 (C), 116.1 (CH), 116.6 (C), 118.3 (CH), 123.3 (CH), 123.5 (2xCH), 125.1 (CH), 128.8 (C), 129.2 (2xCH), 133.1 (C), 136.2 (C), 147.3 (C), 149.7 (C), 150.1 (C), 173.4 (C). LRMS (ESI+) *m/z* (%) 452 $[M+H]^+$ (100). HRMS (ESI+) *m/z* calc. for $C_{24}H_{26}O_6N_3$ 452.1816 $[M+H]^+$, found 452.1808.

*4.1.3. Methyl (1S,3R)-2-(tert-butoxycarbonyl)-1-(4-aminophenyl)- 1,3,4,9-tetrahydropyrido[3,4-b]indole-3-carboxylate (**1**)*

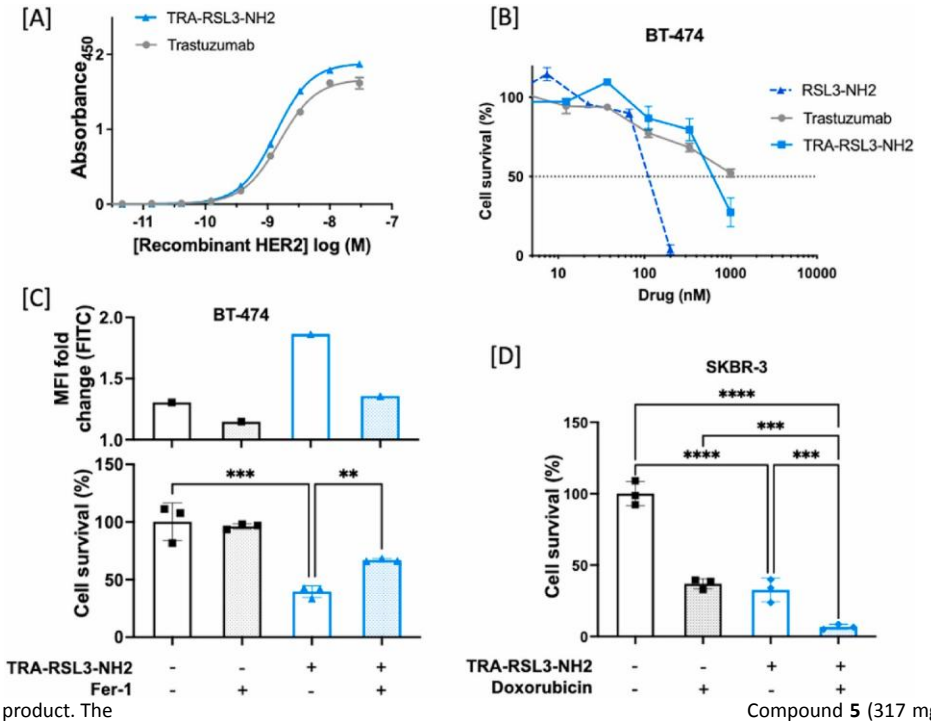

Fig. 5. *In vitro* evaluation of trastuzumab-RSL3-NH_2. [A] HER2 ELISA binding affinity profile of trastuzumab and trastuzumab-RSL3-NH_2. [B] MTT cytotoxicity assay of trastuzumab-RSL3-NH_2, trastuzumab and RSL3 in the HER2-positive BT-474 cancer cell line. Data are presented as a single experiment containing technical replicates, representative of independent experiments. [C] Lipid peroxidation capacity quantification using Bodipy c11 581/591 and cell viability quantification by MTT of BT-474 cancer cells treated with trastuzumab-RSL3-NH_2 (1 and 0.5 µM respectively) alone or in combination with Fer-1 (2 µM) for 72 h. Data are presented as mean + S/D. [D] Cell viability quantification by MTT of SKBR-3 cancer cells treated with trastuzumab-RSL3-NH_2 (1 µM) alone or in combination with doxorubicin (0.025 µM) for 72 h. Data are presented as mean + S/D. Significance was determined ordinary one-way ANOVA, *p < 0.05, **p < 0.01, ***p < 0.001, ****p < 0.0001.

Compound **5** (317 mg, 0.70 mmol) was dissolved in a minimal amount of DCM (2 mL) and diluted with 70 mL of EtOH. The solution was degassed by bubbling argon into the solution during 5 min. Pd/C 10% (70 mg) was added. The flask was purged with H_2 and the reaction mixture was stirred at room temperature under H_2 atmosphere overnight (15 h). After filtration over Celite® to remove the catalyst, the solvent was evaporated under reduced pressure. Purification by column chromatography (DCM/EtOAc 9:1 to 6:4) to obtain the product as a white solid (249 mg, 0.59 mmol, 84% yield). ^{1}H NMR (400 MHz, $CDCl_3$) δ ppm 1.35 (s, 9H), 2.84 (ddd, *J* = 15.9, 11.2, 1.4 Hz, 1H), 3.11 (dd, *J* = 15.9, 4.8 Hz, 1H), 3.63 (dd, *J* = 11.2, 4.8 Hz, 1H), 3.74 (s, 3H), 5.71 (s, 1H), 6.58 (d, *J* = 8.4 Hz, 2H), 6.86 (d, *J* = 8.4 Hz, 2H), 7.24–7.36 (m, 2H), 7.48 (d, *J* = 7.7 Hz, 1H), 8.24 (d, *J* = 8.1 Hz, 1H). ^{13}C NMR (100 MHz, $CDCl_3$) δ ppm 25.8 (CH_2), 27.9 ($3xCH_3$), 49.9 (CH), 52.2 (CH_3), 56.2 (CH), 83.9 (C), 114.9 (2xCH), 115.8 (C), 115.9 (CH), 118.0 (CH), 122.9 (CH), 124.5 (CH), 128.9 (C), 129.2 (2xCH), 132.5 (C), 134.5 (C), 136.6 (C), 145.7 (C), 149.9 (C), 173.9 (C). LRMS (ESI+) *m/z* (%) 422 $[M+H]^+$ (100). HRMS (ESI+) *m/z* calc. for $C_{24}H_{28}O_4N_3$ 422.2074 $[M+H]^+$, found 422.2073.

*4.1.4. 2,5-Dioxopyrrolidin-1-yl 4-azidobutanoate (**6**)*

4-azidobutanoic acid (**S2**, see Supplementary data) (460 mg, 3.56 mmol, 1 eq.), *N*-hydroxysuccinimide (NHS) (533 mg, 4.63 mmol, 1.3 eq.), and EDC.HCl (889 mg, 4.63 mmol, 1.3 eq.) were combined in a flame-dried flask and purged with argon. Dry ACN (4.6 mL) was added via syringe to solubilize the reagents. The reaction mixture was stirred overnight at room temperature. The solvent was removed *in vacuo* and the residue were redissolved in DCM, washed 3 times with water and brine, dried over $MgSO_4$, filtered and concentrated under reduced pressure to give the pure product as a white solid (805 mg, 3.56 mmol, quantitative yield). Spectral data are in accordance with the literature [25].

*4.1.5. N_3-Val-Ala-OH (**2**)*

N_3-Val-Ala-OtBu (**S4**, see Supplementary data) (113 mg, 0.34 mmol) was dissolved in 1.2 mL of anhydrous DCM and the solution was cooled to 0 °C in an ice bath. Trifluoroacetic acid (TFA) (1.2 mL) was added dropwise. When the addition was complete, the ice bath was removed and the reaction mixture was stirred at room temperature for 2 h. The volatiles were evaporated under

reduced pressure to obtain the pure product as a white solid (95 mg, 0.32 mmol, quantitative yield). ^{1}H NMR (400 MHz, CD_3OD) δ ppm 0.96 (d, J = 6.8 Hz, 3H), 0.99 (d, J = 6.8 Hz, 3H), 1.40 (d, J = 7.3 Hz, 3H), 1.82–1.91 (m, 2H), 2.02–2.12 (m, 1H), 2.35 (t, J = 7.4 Hz, 2H), 3.29–3.37 (m, 2H), 4.20 (d, J = 7.3 Hz, 1H), 4.38 (q, J = 7.3 Hz, 1H). ^{13}C NMR (100 MHz, CD_3OD) δ ppm 17.6 (CH_3), 18.7 (CH_3), 19.7 (CH_3), 26.1 (CH_2), 32.0 (CH), 33.7 (CH_2), 49.3 (CH), 51.9 (CH_2), 60.0 (CH), 173.5 (C), 175.1 (C), 175.7 (C). LRMS (ESI-) *m/z* (%) 298 (100) $[M-H]^-$. HRMS (ESI+) *m/z* calc. for $C_{12}H_{22}O_4N_5$ 300.1666 $[M+H]^+$, found 300.1668.

*4.1.6. N_3-Val-Ala-(Boc)RSL3-NH_2 (**7**)*

Compound **2** (45 mg, 0.150 mmol, 1 eq.), HATU (86 mg, 0.230 mmol, 1.5 eq.), pyridine (12 mg, 0.150 mmol, 1 eq.) were dissolved in anhydrous DCM (3 mL) and DMF (3 mL). After 10 min, this mixture was added to a flask containing **1** (63 mg, 0.150 mmol, 1 eq.) under argon atmosphere. The reaction mixture was stirred at room temperature overnight. Water was added to the reaction mixture. The resulting mixture was extracted 3 times with DCM. The combined organic layers were washed with water and brine, dried over $MgSO_4$ and evaporated. The crude product was triturated and precipitated in Et_2O to obtain the pure product as a white solid (72 mg, 68% yield).The product was further purified by column chromatography (DCM/MeOH 99:1 to 97:3). ^{1}H NMR (400 MHz, $CDCl_3$) δ ppm 0.89 (d, J = 7.1 Hz, 3H), 0.91 (d, J = 7.1 Hz, 3H), 1.34 (s, 9H), 1.43 (d, J = 6.9 Hz, 3H), 1.83–1.95 (m, 2H), 1.96–2.09 (m, 1H), 2.30–2.46 (m, 2H), 2.84 (dd, J = 15.8, 11.3 Hz, 1H), 3.11 (dd, J = 15.8, 4.7 Hz, 1H), 3.21–3.29 (m, 2H), 3.57 (dd, J = 11.0, 4.8 Hz, 1H), 3.72 (s, 3H), 4.48–4.57 (dd, J = 8.1, 8.1 Hz, 1H), 4.77–4.89 (m, 1H), 5.77 (s, 1H), 6.87 (d, J = 8.6 Hz, 1H), 7.05 (d, J = 8.4 Hz, 2H), 7.24–7.36 (m, 3H), 7.44–7.52 (m, 3H), 7.65 (d, J = 6.8 Hz, 1H), 8.22 (d, J = 8.1 Hz, 1H), 8.91 (bs, 1H). ^{13}C NMR (100 MHz, $CDCl_3$) δ ppm 18.1 (CH_3), 18.5 (CH_3), 19.1 (CH_3), 24.9 (CH_2), 25.6 (CH_2), 27.9 (3xCH_3), 31.6 (CH), 33.2 (CH_2), 49.5 (CH), 49.9 (CH), 50.7 (CH_2), 52.2 (CH_3), 56.0 (CH), 58.3 (CH), 84.0 (C), 115.8 (C), 116.0 (CH), 118.0 (CH), 119.6 (2xCH), 122.9 (CH), 124.6 (CH), 128.7 (2xCH), 128.8 (C), 133.9 (C), 136.4 (C), 137.1 (C), 138.4 (C), 149.7 (C), 170.5 (C), 171.7 (C), 172.4 (C), 173.6 (C). LRMS (ESI+) *m/z* (%) 507 (50), 703 (100) $[M+H]^+$, 725 (25) $[M+Na]^+$. HRMS (ESI+) *m/z* calc. for $C_{36}H_{47}O_7N_8$ 703.3562 $[M+H]^+$, found 703.3539.

*4.1.7. N_3-Val-Ala-RSL3-NH_2 (**8**)*

N_3-Val-Ala-(NH)RSL3-NH_2 (**S5,** see Supplementary data) (138 mg, 0.23 mmol, 1 eq.) was dissolved in 0.5 mL anhydrous DMF, then 4.0 mL of anhydrous DCM was added. The solution was cooled to 0 °C in an ice bath before addition of Et_3N (0.06 mL, 0.46 mmol, 2.0 eq.). To this mixture was added dropwise chloroacetyl chloride (0.03 mL, 0.34 mmol, 1.5 eq.) diluted in 0.5 mL of anhydrous DCM. The mixture was stirred under argon atmosphere from 0 °C to room temperature overnight. The reaction mixture was diluted with DCM and water was added. The mixture was extracted 3 times with DCM, the combined organic layers were washed with brine, dried over Na_2SO_4 and concentrated. The final product was purified by column chromatography (DCM/MeOH 99:1 to 97:3) to obtain the pure product as a white solid (139 mg, 0.20 mmol, 89% yield). ^{1}H NMR (400 MHz, DMSO-d_6) δ ppm 0.82 (d, J = 6.8 Hz, 3H), 0.86 (d, J = 6.8 Hz, 3H), 1.27 (d, J = 6.6 Hz, 3H), 1.68–1.80 (m, 2H), 1.89–2.01 (m, 1H), 2.18–2.31 (m, 2H), 3.30 (t, J = 7.3 Hz, 2H), 3.15–3.64 (m, 6H), 4.10–4.41 (m, 3H), 4.69 (d, J = 14.0 Hz, 1H), 5.27–6.33 (m, 1H), 6.88–7.71 (m, 8H), 7.90 (d, J = 8.6 Hz, 1H), 8.14 (bs, 1H), 9.76–10.00 (m, 1H), 10.77–11.08 (m, 1H). ^{13}C NMR (100 MHz, DMSO-d_6) δ ppm 18.0 (CH_3), 18.1 (CH_3), 19.2 (CH_3), 21.6 (CH_2), 24.6 (CH_2), 30.4 (CH), 32.0 (CH_2), 42.8 (CH_2), 48.9 (CH), 50.3 (CH_2), 53.0 (CH), 53.9 (CH_3), 55.8 (CH), 57.6 (CH), 111.3 (CH), 117.9 (CH), 118.8–121.2 (5xCH), 125.5–125.8 (1xC, 2xCH), 135.2–136.4 (3xC), 167.6 (C), 170.9–171.2 (3xC), 171.6 (C). LRMS (ESI+) *m/z* (%) 507 (25), 679 (80) $[M+H]^+$, 701 (100) $[M+Na]^+$. HRMS (ESI+) *m/z* calc. for $C_{33}H_{39}ClO_6N_8Na$ 701.2573 $[M+Na]^+$, found 701.2563.

4.1.8. Bioconjugation

*4.1.8.1. Preparation of the trastuzumab-DBCO conjugate (**3**).* To 1 mL of the solution of trastuzumab (5 mg/mL) in PBS (1X, pH 7.4) containing EDTA (2 mM) was added a solution of TCEP (6.67 µL, 10 eq., 50 mM) in water. The resulting mixture was briefly vortexed and then incubated at 37 °C for 2 h, allowing for the reduction of interchain disulfide bonds. To the resulting solution of the reduced antibody was added a solution of maleimide-PEG4-DBCO (33.3 µL, 10 eq., 10 mM) in DMSO. The mixture was incubated at room temperature for 1 h. The conjugate was purified using Amicon 30K.

4.1.8.2. Preparation of trastuzumab-RSL3-NH_2 conjugates. To the solution of **3** (5 mg/mL) in PBS (1X, pH 7.4) was added a solution of **8** (33.3 µL, 10 eq., 10 mM) in DMSO. The mixture was incubated at 25 °C for 16 h. The RSL3-based conjugates were purified 3 times in PBS 7.4 using Amicon 30K centrifugal filter. Final antibody-drug conjugate concentration was measured at 280 nm using a NanoDrop™ One spectrophotometer (ThermoScientific). The two ADCs that were tested are >95% pure by HPLC analysis.

4.1.8.3. Physico-chemical characterization of antibody-drug conjugates. Denaturing Reversed Phase Chromatography—Mass Spectrometry (RPLC-MS) was performed on a Thermo UltiMate 3000 UHPLC system + Bruker Impact II™ Q-ToF mass spectrometer. Mobile phase A was water +0.1% formic acid and mobile phase B was acetonitrile +0.1% formic acid. Column was an Agilent PLRP-S 1000 Å 2.1 × 150 mm 8 µm (80 °C). Gradient was 20 %B to 50 %B in 25 min. Flow rate was 0.4 ml/ min. UV detection was monitored at 280 nm. The Q-ToF mass spectrometer was used in the *m/z* range 500–3500 (ESI+). Data were deconvoluted using the MaxEnt algorithm included in the Bruker Compass® software. mAb or ADC samples were diluted with H_2O for injection (approx. 1.5 mg/ml final ADC concentration).

Size Exclusion Chromatography (SEC) was performed on an Agilent 1100 HPLC system having an extra-column volume below 15 µl (equipped with short sections of 0.12 mm internal diameter peek tubing and a micro-volume UV flow cell). Column was an Agilent AdvanceBioSEC 300 Å 4.6 × 150mm 2.7 µm (maintained at 30 °C). Mobile phase was 100 mM sodium phosphate and 200 mM sodium chloride (pH 6.8). 10% acetonitrile (v/v) was added to the mobile phase to minimize secondary hydrophobic interactions with the stationary phase and prevent bacterial growth. Flow rate was 0.35 ml/min. UV detection was monitored at 220 and 280 nm.

4.2. Biology

4.2.1. Cell culture

HER2-positive human breast adenocarcinoma cell lines BT-474 and SKBR-3, gastric cancer cell line NCI–N87 and esophageal cancer cell line OE-19 were cultured in RPMI medium supplemented with 10% fetal calf serum and 100 µg/ml streptomycin. Blood cancer cell lines Toledo, MOLM-13, MM.1S, HEL, HL-60 and Karpas-422 were cultured in RPMI medium supplemented with 10% fetal calf serum and 100 µg/ml streptomycin. All cell lines were maintained at 37 °C, under 5% CO_2 atmosphere.

4.2.2. Chemicals

(1*S*,3*R*)-RSL3 was purchased from TOCRIS (6118), ferrostatin-1 was purchased from Abcam (Ab146169), and doxorubicin was purchased from TEVA.

4.2.3. Western blots

10.10^6 cells were harvested, and protein were extracted using complete RIPA buffer (RIPA buffer, 1 mM DTT, 1 M NaF, 100 mM sodium orthovanadate, phosphatase inhibitor buffer and protease inhibitors) for 1 h in ice. Lysate were centrifuged 15 min at 12000×*g* at 4 °C. 50 µg of proteins were mixed with 4x Laemmli Sample Buffer (Bio-Rad), heated at 95 °C for 5 min and separated by SDS PAGE (PROTEAN TGX Stain- Free Gels, Bio-Rad). Proteins were then transferred onto PVDF membrane (iBlot®2 PVDF stacks,

Invitrogen) using the iBlot2 device (Invitrogen) and blocked with TBS buffer (Intercept® Blocking Buffer, LI- COR). Primary antibodies were incubated overnight at 4 °C and secondary antibodies (IRDye Infrared Dyes from LI-COR Biosciences) 1 h at room temperature. Primary antibody used were: anti-GPX4 (Ab41787, Abcam, 1:1000) and anti-β-actin (A5441, Sigma-Aldrich, 1:5000). Membranes were scanned using the c500 Azure Biosystem (Ozyme) and densitometric quantification were performed using ImageJ software. Protein levels were normalized against β-actin.

4.2.4. In vitro cytotoxicity assays

Cells were plated at the appropriate density by adding 100 µl/well of cell solution in 96-well plates. Serial 3-fold dilutions of the tested compound were added, and plates were incubated at 37 °C, 5% CO_2 for 3–6 days. MTT (5 mg/ml, 20 µl, Sigma-Aldrich) was added into the wells, and incubation was carried for 2-to-4 hours at 37 °C. Culture media was then carefully removed, and formazan crystals were homogeneously dissolved with 0.1 N HCl/isopropanol. Absorbance values were measured on a Thermo Scientific Multiskan™ EX microplate reader using a wavelength of 570 nm (with a reference wavelength of 690 nm). The IC_{50} concentration values compared to untreated control cells were determined using inhibition dose response curve fitting (GraphPad Prism 9).

4.2.5. In vitro combination assays

Cells were plated at the appropriate density by adding 100 µl/well of cell solution in 96-well plates. Cells were exposed to either the treatment alone or the combination for 2 or 9 days depending on the combination assay (ferrostain-1 combination or doxorubicin combination respectively). MTT (5 mg/ml, 20 µl/well, Sigma-Aldrich) was added into the wells, and incubation was carried for 2-to-4 hours at 37 °C. Culture media was then carefully removed, and formazan crystals were homogeneously dissolved with 0.1 N HCl/isopropanol. Absorbance values were measured on a Thermo Scientific Multiskan™ EX microplate reader using a wavelength of 570 nm (with a reference wavelength of 690 nm). The cell survival percentages were calculated compared to untreated control wells.

4.2.6. PAMPA assay

Passive permeabilities of RSL3 and RSL3-NH_2 were compared by parallel artificial membrane permeability assay (PAMPA assay) as described before [19], using a GenTest™ pre-coated PAMPA plate system (Corning®), following manufacturer's protocol and calculation procedures. The assay buffer was PBS 7.4 + 10% MeOH (v/v). The initial compound concentration in the donor compartment was 100 µM. Residual DMSO in the assay was kept below 1% (v/v). The permeability partitioning was realized for 5 h at room temperature while stirring the plate at 300 rpm on a Heidolph Titramax 101 device. Final concentration of tested compound in the donor and acceptor compartments was assessed by HPLC-UV, against known calibration curves of compounds.

4.2.7. Reactive oxygen species (ROS) quantification

BT-474 cells were plated at 8000 cells/well, 100 µl/well and incubated overnight at 37 °C, 5% CO_2, then treated with RSL3 (1 µM), RSL3- NH_2 (10 µM) or co-treated with ferrostain-1 (20 µM) or doxorubicin (1 µM) for 1 h 37 °C, 5% CO_2. Treatments were then removed, and cells were washed using DPBS and incubated with 10 µM of H2D-CFDA in DPBS for 30 min at 37 °C. Fluorescence intensity were measured using the Chameleon multilabel microplate reader (Hidex) and ROS induction ratio were calculated compared to untreated but H2D-CFDA-stained control wells.

4.2.8. Sandwich ELISA binding assay

96-well high-binding ELISA plates (Corning Inc.) were coated by adding 100 µl/well of trastuzumab or trastuzumab-RSL3-NH_2 at 2 µg/ml (PBS 7.4) in replicates and incubated overnight at 4 °C. After two washes with PBS-T (PBS 7.4, 0.05% Tween-20), the plate was blocked with 200 µl/well of incubation buffer (PBS-T, 0.1% BSA) for 1 h at room temperature, then washed 4 times with PBS-T and 100 µl of a 3-fold dilution series of His-tagged HER2 recombinant protein (Sino Biological Inc.) prepared in incubation buffer were added and incubated for 2 h at room temperature in the dark. The plate was then washed 5 times with PBS-T, incubated 1 h at room temperature with 100 µl/well of HRP-conjugated anti-His Tag secondary antibody (Takara Inc., 1:5000), washed 5 times with PBS-T, and incubated with TMB substrate solution (Thermo-Fisher) for 12 min. Peroxidase activity was stopped with 0.18 M H_2SO_4 and absorbance was read at 450 nm (reference wavelength 650 nm) using a Thermo Scientific MultiSkan™ EX microplate reader. Sigmoidal fittings were performed using GraphPad Prism 9 software.

4.3. Statistical analyses

Statistical p-values were calculated using ordinary one-way ANOVA or nonparametric Mann-Whitney t-tests and performed using GraphPad Prism 9 software.

Declaration of competing interest

The authors declare that they have no known competing financial interests or personal relationships that could have appeared to influence the work reported in this paper.

Data availability

Data will be made available on request.

Acknowledgements

K.-A.N and A.B thank the French Research Agency (ANR) for the financial support (grant CLAMP2). L.C is supported by the French National Association of Research and Technology (ANRT). A.B is thankful to the CBH-EUR-GS (ANR-17-EURE-0003) for the financial support.

Appendix A. Supplementary data

Supplementary data to this article can be found online at https://doi.org/10.1016/j.ejmech.2022.114863.

References

[1] S.J. Dixon, K.M. Lemberg, M.R. Lamprecht, R. Skouta, E.M. Zaitsev, C.E. Gleason, D.N. Patel, A.J. Bauer, A.M. Cantley, W.S. Yang, B. Morrison 3r, B.R. Stockwell, Ferroptosis: an iron-dependent form of nonapoptotic cell death, Cell 149 (2012) 1060–1072, https://doi.org/10.1016/j.cell.2012.03.042.

[2] W.S. Yang, R. Sriramaratnam, M.E. Welsch, K. Shimada, R. Skouta, V. S. Viswanathan, J.H. Cheah, P.A. Clemons, A.F. Shamji, C.B. Clish, L.M. Brown, A. W. Girotti, V.W. Cornish, S.L. Schreiber, B.R. Stockwell, Regulation of ferroptotic cancer cell death by GPX4, Cell 156 (2014) 317–331, https://doi.org/10.1016/j. cell.2013.12.010.

[3] W.S. Yang, K.J. Kim, M.M. Gaschler, M. Patel, M.S. Shchepinov, B.R. Stockwell, Peroxidation of polyunsaturated fatty acids by lipoxygenases drives ferroptosis, Proc. Natl. Acad. Sci. U.S.A. 113 (2016) E4966–E4975, https://doi.org/10.1073/ pnas.1603244113.

[4] A. Borchert, J. Kalms, S.R. Roth, M. Rademacher, A. Schmidt, H.G. Holzhutter, H. Kuhn, P. Scheerer, Crystal structure and functional characterization of selenocysteine-containing glutathione peroxidase 4 suggests an alternative mechanism of peroxide reduction, Biochim. Biophys. Acta, Mol. Cell Biol. Lipids 1863 (2018) 1095–1107, https://doi.org/10.1016/j.bbalip.2018.06.006.

[5] M.J. Hangauer, V.S. Viswanathan, M.J. Ryan, D. Bole, J.K. Eaton, A. Matov, J. Galeas, H.D. Dhruv, M.E. Berens, S.L. Schreiber, F. McCormick, M.T. McManus, Drug-tolerant persister cancer cells are vulnerable to GPX4 inhibition, Nature 551 (2017) 247–250, https://doi.org/10.1038/nature24297.

[6] J.P.F. Angeli, R. Shah, D.A. Pratt, M. Conrad, Ferroptosis inhibition: mechanisms and opportunities, Trends Pharmacol. Sci. 38 (2017) 489–498, https://doi.org/ 10.1016/j.tips.2017.02.005.

[7] D. Moosmayer, A. Hilpmann, J. Hoffmann, L. Schnirch, K. Zimmermann, V. Badock, L. Furst, J.K. Eaton, V.S. Viswanathan, S.L. Schreiber, S. Gradl, R. C. Hilling, Crystal structures of the selenoprotein glutathione peroxidase 4 in its apo form and in complex with the covalently bound inhibitor ML162, Acta Crystallogr. Sect. D Struct. Biol. 77 (2021) 237–248, https://doi.org/10.1107/ S2059798320016125.

[8] W.S. Yang, B.R. Stockwell, Synthetic lethal screening identifies compounds activating iron-dependent, nonapoptotic cell death in oncogenic-RAS-harboring cancer cells, Chem. Biol. 15 (2008) 234–245, https://doi.org/10.1016/j. chembiol.2008.02.010.

[9] M. Weïwer, J.A. Bittker, T.A. Lewis, K. Shimada, W.S. Yang, M.L. Dandapani, M. Palmer, B.R. Stockwell, S.L. Schreiber, B. Munoz, Development of small- molecule probes that selectively kill cells induced to express mutant RAS, Bioorg. Med. Chem. Lett. 22 (2012) 1822–1826, https://doi.org/10.1016/j. bmcl.2011.09.047.
[10] J.K. Eaton, R.A. Ruberto, A. Kramm, V.S. Viswanathan, S.L. Schreiber, Diacylfuroxans are masked nitrile oxides that inhibit GPX4 covalently, J. Am. Chem. Soc. 141 (2019) 20407–20415, https://doi.org/10.1021/jacs.9b10769.
[11] J.K. Eaton, L. Furst, R.A. Ruberto, D. Moosmayer, A. Hilpmann, M.J. Ryan, K. Zimmermann, L.L. Cai, M. Niehues, V. Badock, A. Kramm, S. Chen, R.C. Hillig, P. A. Clemons, S. Gradl, C. Montagnon, K.E. Lazarski, S. Christian, B. Bajrami, R. Neuhaus, A.L. Eheim, V.S. Viswanathan, S.L. Schreiber, Selective covalent targeting of GPX4 using masked nitrile-oxide electrophiles, Nat. Chem. Biol. 16 (2020) 497–506, https://doi.org/10.1038/s41589-020-0501-5.
[12] J.K. Eaton, L. Furst, L.L. Cai, V.S. Viswanathan, S.L. Schreiber, Structure–activity relationships of GPX4 inhibitor warheads, Bioorg. Med. Chem. Lett. 30 (2020), 127538, https://doi.org/10.1016/j.bmcl.2020.127538.
[13] J.M. Lambert, A. Berkenblit, Antibody-drug conjugates for cancer treatment, Annu. Rev. Med. 69 (2018) 191–207, https://doi.org/10.1146/annurev-med-061516- 121357.
[14] N. Joubert, A. Beck, C. Dumontet, C. Denevault-Sabourin, Antibody-drug conjugates: the last decade, Pharmaceuticals 13 (2020) 1–30, https://doi.org/ 10.3390/ph13090245.
[15] H. Yao, F. Jiang, A. Lu, G. Zhang, Methods to design and synthesize antibody-drug conjugates (ADCs), Int. J. Mol. Sci. 17 (2016) 194, https://doi.org/10.3390/ijms17020194.
[16] S.C. Jeffrey, P.J. Burke, R.P. Lyon, D.W. Meyer, D. Sussman, M. Anderson, J. H. Hunter, C.I. Leiske, J.B. Miyamoto, N.D. Nicholas, N.M. Okeley, R.J. Sanderson, I.J. Stone, W. Zeng, S.J. Gregson, L. Masterson, A.C. Tiberghien, P.W. Howard, D. E. Thurston, C.-L. Law, P.D. Senter, Potent anti-CD70 antibody-drug conjugate combining a dimeric pyrrolobenzodiazepine drug with site-specific conjugation Technology, bioconjug, Chem 24 (2013) 1256–1263, https://doi.org/10.1021/ bc400217g.
[17] J. Magano, B.G. Conway, D. Farrand, M. Lovdahl, M.T. Maloney, M.J. Pozzo, J. J. Teixeira, J. Rizzo, D. Tumelty, Scalable and cost-effective synthesis of a linker for bioconjugation with a peptide and a monoclonal antibody, Synthesis 46 (2014) 1399–1406, https://doi.org/10.1055/s-0033-1340980.
[18] S.J. Walsh, J.D. Bargh, F.M. Dannheim, A.R. Hanby, H. Seki, A.J. Counsell, X. Ou, E. Fowler, N. Ashman, Y. Takada, A. Isidro-Llobet, J.S. Parker, J.S. Caroll, D. R. Spring, Site-selective modification strategies in antibody–drug conjugates, Chem. Soc. Rev. 50 (2021) 1305–1353, https://doi.org/10.1039/D0CS00310G.
[19] L. Conilh, G. Fournet, E. Fourmaux, A. Murcia, E.-L. Matera, B. Joseph, C. Dumontet, W. Viricel, Exatecan antibody drug conjugates based on a hydrophilic polysarcosine drug-linker platform, Pharmaceuticals 14 (2021) 247, https://doi. org/10.3390/ph14030247.
[20] A.I. Fraguas-Sanchez, I. Lozza, A.I. Torres-Su´ arez, Actively targeted nanomedicines ´ in breast cancer: from pre-clinal investigation to clinic, Cancers 14 (2022) 1198, https://doi.org/10.3390/cancers14051198.
[21] J.L. Roh, E.H. Kim, H. Jang, D. Shin, Nrf2 inhibition reverses the resistance of cisplatin-resistant head and neck cancer cells to artesunate-induced ferroptosis, Redox Biol. 11 (2017) 254–262, https://doi.org/10.1016/j.redox.2016.12.010.
[22] X. Zhang, S. Sui, L. Wang, H. Li, L. Zhang, S. Xu, X. Zheng, Inhibition of tumor propellant glutathione peroxidase 4 induces ferroptosis in cancer cells and enhances anticancer effect of cisplatin, J. Cell. Physiol. 35 (2020) 3425–3437, https://doi.org/10.1002/jcp.29232.
[23] J. Ye, X. Jiang, Z. Dong, S. Hu, M. Xiao, Low-concentration PTX and RSL3 inhibits tumor cell growth synergistically by inducing ferroptosis in mutant p53 hypopharyngeal squamous carcinoma, Cancer Manag. Res. 11 (2019) 9783–9792, https://doi.org/10.2147/CMAR.S217944.
[24] B. Hassania, P. Vandenabeele, T. Vanden Beghe, Targeting ferroptosis to iron out cancer, Cancer Cell 35 (2019) 830–849, https://doi.org/10.1016/j. ccell.2019.04.002.
[25] B.A. Badeau, M.P. Comerford, C.K. Arakawa, J.A. Shadish, C.A. DeForest, Engineered modular biomaterial logic gates for environmentally triggered therapeutic delivery, Nat. Chem. 10 (2018) 251–258, https://doi.org/10.1038/ nchem.2917.